European Journal of Pharmaceutics and Biopharmaceutics 75 (2010) 33–41

Contents lists available at ScienceDirect

European Journal of Pharmaceutics and Biopharmaceutics

journal homepage: www.elsevier.com/locate/ejpb

Research paper

Comparison of bioavailability of amorphous versus crystalline itraconazole nanoparticles via pulmonary administration in rats

Wei Yang [a,1], Keith P. Johnston [b,*], Robert O. Williams III [a,*]

[a] Division of Pharmaceutics, University of Texas at Austin, Austin, TX, USA
[b] Department of Chemical Engineering, University of Texas at Austin, Austin, TX, USA

ARTICLE INFO

Article history:
Received 14 July 2009
Accepted in revised form 20 January 2010
Available online 25 January 2010

Keywords:
Poorly water-soluble drug
Aerosol
Supersaturation
Nebulization
Inhalation
Lung
Pharmacokinetics
In vivo

ABSTRACT

The effect of supersaturation on bioavailability of inhaled nebulized aerosols is compared for amorphous versus crystalline nanoparticulate dispersions. The nanocrystalline formulations of itraconazole (ITZ) were made by wet milling (*i.e.* Wet-milled ITZ), whereas amorphous nanostructured aggregates (ITZ/mannitol/lecithin = 1:0.5:0.2, weight ratio) were made by an ultra-rapid freezing process (*i.e.* URF–ITZ). Dissolution tests revealed the extent of supersaturation was 4.7-times higher for URF–ITZ versus Wet-milled ITZ, though their dissolution rates were similar. The aerodynamic performances of both aqueous colloidal dispersions were comparable and suitable for deep lung delivery. Single-dose 24-h pharmacokinetic studies were conducted in Sprague–Dawley rats following inhalation of the nebulized colloidal dispersions (equivalent to 20 mg ITZ/mL dispersion in 5 mL) in a nose-only dosing apparatus. Lung depositions following inhalation were similar for both compositions. In systemic circulation, Wet-milled ITZ and URF–ITZ achieved C_{max} of 50 and 180 ng/mL at 2.7 and 4.0 h, and AUC_{0-24} of 662 and 2543 ng h/mL, respectively, based on a one-compartmental analysis. Pulmonary delivery of the nanoparticulate amorphous ITZ composition resulted in significantly higher systemic bioavailability than for the nanocrystalline ITZ composition, as a result of the higher supersaturation that increased the permeation.

© 2010 Elsevier B.V. All rights reserved.

1. Introduction

Modern drug discovery processes, which routinely use high-throughput screening techniques, appear to result in a higher prevalence of lead compounds of increased molecular weight and lipophilicity [1,2]. Such drug molecules pose challenges to formulate therapeutically effective products for clinical use, since they often have poor bioavailability issues due to their poor dissolution or poor permeability to achieve sufficient and consistent systemic exposure. Consequently, it results in sub-optimal efficacy in patients, particularly when delivered via the oral administration [3,4].

To address the issues of low aqueous solubility, solubilization and micronization have commonly been used to increase dissolution rate and thereby oral bioavailability of such drugs. Attempts to solubilize and stabilize these drugs using salt formation [5], co-solvents [6], micellar solutions [7], and inclusion complexes with cyclodextrins [8] have been of limited success. The increased amount of excipients required to formulate the poorly water-soluble drugs may potentially increase side effects, resulting in low patient compliance. Alternatively, invasive dosage forms such as parenteral formulations have to be developed to address the challenges. However, with even less pharmaceutically acceptable excipient options, solubilization of drug is practically limited [9].

For the means of micronization, although particle size reduction of the poorly water-soluble drugs increases their dissolution rate by increased surface area, it does not increase equilibrium solubility. Often for drugs with very low aqueous solubility, the achieved increase in dissolution rate is limited and insufficient to provide significant enhancement of bioavailability [3].

However, drug particles in the 100-nm range dissolve more quickly and to a greater extent (*i.e.*, higher equilibrium solubility) than for micronized drug particles, as described by the Noyes–Whitney and Ostwald–Freundlich equations [10]. Both particle dissolution kinetics and solubility are size dependent. Thus, the dissolution of drug nanoparticles *in vivo* is usually accompanied by an increase in bioavailability [11,12]. On the other hand, the potential for increased Van der Waals interactions and electrostatic attraction between ultrafine particles can reduce the effective surface area for dissolution and therefore counteract improvements in

* Corresponding authors. The University of Texas at Austin, Department of Chemical Engineering, 1 University Station, Mail Stop C0400, Austin, TX 78712, USA. Tel.: +1 512 471 4617; fax: +1 512 471 7060 (K.P. Johnston); The University of Texas at Austin, College of Pharmacy, 1 University Station, Mail Stop A1920, Austin, TX 78712, USA. Tel.: +1 512 471 4681; fax: +1 512 471 7474 (R.O. Williams).
E-mail addresses: weiyang@mail.utexas.edu (W. Yang), kpj@che.utexas.edu (K.P. Johnston), williro@mail.utexas.edu (R.O. Williams).
[1] Tel.: +1 512 471 7886; fax: +1 512 471 7474.

0939-6411/$ - see front matter © 2010 Elsevier B.V. All rights reserved.
doi:10.1016/j.ejpb.2010.01.011

bioavailability [13]. Colloidal dispersions of drug nanocrystals with a typical mean particle size between 200 and 500 nm and stabilized by a suitable stabilizer (*i.e.* nanosuspension) [4] have therefore been developed as an alternative approach.

The effectiveness of nanosuspensions of poorly water-soluble drugs in enhancing bioavailability has been proved in animal models and clinical trials with various administration routes, including oral [14,15], pulmonary [16,17], ocular [18,19], and parenteral delivery due to their particle size sufficiently small to be injected intravenously [20,21]. Among these, of particular interest is inhalation delivery, because of the following advantages of this noninvasive delivery route: (1) Potential for high systemic absorption with an enormous absorptive surface area of averagely 100 m^2, very thin diffusion path to the blood stream and rich vasculature that facilitate rapid delivery of large drug doses. (2) Targeted local lung action with reduced systemic side effects relative to other routes of administration. (3) Relatively low metabolic activity and avoidance of hepatic first-pass metabolism [22].

Several studies predicted from thermodynamics the potential impact of polymorphs on bioavailability based on *in vitro* dissolution profiles and/or thermal analysis for oral delivery [23,24]. The amorphous form of a drug has a higher thermodynamic chemical potential than its crystalline counterpart [25]. The higher thermodynamic activity of the drug can produce supersaturated solutions [26,27], thereby providing an opportunity to enhance absorption and bioavailability. In most experimental studies, supersaturation values of micron-sized particles are less than 5, despite predictions from calorimetric measurements of the heat capacity (used to determine the free energy) that they can be much larger [23,28]. Significantly higher supersaturation values approaching 100 was achieved for amorphous nanoparticles relative to microparticles, as the microparticles crystallize in the solid state before they dissolve and produce high supersaturation [29].

Amorphous nanostructured formulations of poorly water-soluble drugs for pulmonary delivery have also been developed to enhance therapeutic effectiveness [30,31]. Vaughn et al. reported that inhalation of nebulized aerosols of ITZ amorphous nanoparticulate composition (ITZ/polysorbate 80/poloxamer 407 = 1:0.75:0.75, w/w/w, named SFL-ITZ) into mice for 20 min, achieved a lung tissue C_{max} of 13.4 μg/g wet lung weight and AUC_{inf} of 99.7 μg h/mL, and serum C_{max} of 0.12 μg/mL [32]. Inhalation of a crystalline ITZ nanostructured composition (ITZ/poloxamer 407/polysorbate 80 = 1:0.16:0.13, w/w/w, named EPAS-ITZ) in the same mice model produced high lung C_{max} of 16.8 μg/g wet lung weight and AUC_{inf} of 85.8 μg h/mL, but no systemic ITZ level was reported [33]. Despite the similar lung depositions of inhaled ITZ, in a subsequent prophylaxis study using a mouse model of invasive pulmonary aspergillosis, the nebulized aerosols of SFL-ITZ led to higher survival than for EPAS-ITZ for both short (8 days) and long-term survival (20 days) [34]. This improvement in survival may result from a higher supersaturation of ITZ in the lung fluid for the amorphous SFL-ITZ, compared to crystalline EPAS-ITZ formulation.

To our knowledge, so far no study assessed the effects of amorphous versus crystalline nanoparticulate formulations of a poorly water-soluble drug on *in vivo* bioavailability following lung delivery. In the present study, we evaluate the impact of the *in vitro* solubility advantage of amorphous versus crystalline nanoparticulate formulations of poorly water-soluble drug on *in vivo* bioavailability following pulmonary administration. We hypothesize that the supersaturation produced by inhaled amorphous nanoparticles of a poorly water-soluble drug will produce a higher systemic absorption and thereby enhanced bioavailability, relative to the nanocrystalline counterpart bioavailability. ITZ was chosen as a model poorly water-soluble drug, because of its extremely high lipophilicity, *i.e.* an estimated aqueous solubility of about 1 ng/mL at neutral pH and a calculated *Clog P* value of 6.2 [35]. A nano-sized crystalline ITZ composition was made by wet ball milling process (*i.e.* Wet-milled ITZ). The amorphous nanostructured aggregates of ITZ composition (ITZ/mannitol/lecithin = 1:0.5:0.2, w/w/w) with a large, wettable surface made by ultra-rapid freezing process (*i.e.* URF–ITZ) were reported previously [31]. We compare both the physiochemical properties *in vitro* and the bioavailability after inhalation in rats. Given that pulmonary delivery has become an increasingly attractive route of application for poorly water-soluble drugs, the ability to provide greater insight into formulation design for improved bioavailability will be of widespread interest.

2. Materials and methods

2.1. Materials

The following materials were purchased: ITZ, micronized B.P. grade (Hawkins Chemical, Minneapolis, MN); mannitol and lecithin (Spectrum Chemicals, Gardena, CA); 1,4-dioxane and acetonitrile (Fisher Scientific, Fair Lawn, NJ); diethanolamine (VWR International, West Chester, PA). All organic solvents used were HPLC grade. Other reagents used were at least of ACS grade.

2.2. Preparation of crystalline ITZ nanoparticulates and amorphous nanostructured aggregate of ITZ

The crystalline ITZ nanoparticulates were prepared by wet ball milling in a ceramic jar with Zirconia grinding media (1/2″ Radius end cylinder) (US Stoneware, East Palestine, OH). Three grams of the commercially available ITZ powder (mean particle size of 5 μm in diameter, 100% < 17.7 μm) was added to 15 mL of purified water and milled at 100 rpm 20 °C under nitrogen gas for 10 days. Thus obtained slurry was combined with several successive washings of the ceramic jar and milling media using purified water to make a dispersion of the milled ITZ, which was then quickly frozen by dripping into liquid nitrogen and lyophilized to obtain dry powder by using a VirTis Advantage bench top tray lyophilizer (The VirTis Company, Inc., Gardiner, NY, USA). The obtained Wet-milled ITZ dry powder was stored in a desiccator under vacuum (~15% relative humidity) at room temperature.

Amorphous nanostructured aggregate URF–ITZ powder was prepared using the ultra-rapid freezing (URF) technology, as described previously [31]. In brief, lecithin was dissolved in a mixture of 1,4-dioxane and purified water (65/35, v/v) co-solvent system using a magnetic stirrer. Mannitol and ITZ were subsequently dissolved in the mixture, in a weight ratio of ITZ/mannitol/lecithin = 1:0.5:0.2. The solution was rapidly frozen after applied to the URF apparatus that pre-cooled to about −70 °C [36]. The frozen solids were collected, lyophilized, and stored the same as described for Wet-milled ITZ dry powder.

2.3. Scanning electron microscopy (SEM)

SEM was used to evaluate the morphology of the samples. The samples were coated using a model K575 sputter coater (Emitech Products, Inc., Houston, TX) with gold/palladium for 20 s in a high vacuum evaporator. SEM was performed using a Hitachi S-4500 field emission scanning electron microscope (Hitachi High-Technologies Corp., Tokyo, Japan) operating at an accelerating voltage of 10–15 kV. Images were captured with Quartz PCI software (Quartz Imaging Corporation, Vancouver, BC, Canada).

2.4. Powder X-ray diffraction (XRD)

The crystallinity of the dried powders of Wet-milled ITZ and URF–ITZ was examined by wide angle XRD. A Philips 1710 X-ray

diffractometer with a copper target (Cu Ka1, λ = 1.54056 Å) and nickel filter (Philips Electronic Instruments Inc., Mahwah, NJ) was used to obtain the XRD patterns. Samples were analyzed in the 2-theta range from 10° to 50° using a step size of 0.05 2-theta degree with a dwell time of 2 s.

2.5. Modulated temperature differential scanning calorimetry (MTDSC)

Thermal properties of the powder samples were investigated using a TA Instruments Model 2920 DSC (New Castle, DE), equipped with a refrigerated cooling system. Dry nitrogen gas was used as the purge gas through the DSC cell at a flow rate of 40 mL/min. Samples were weighed to 10–15 mg in aluminum crimped pans (Kit 0219-0041, Perkin–Elmer Instruments, Norwalk, CT). The mass of the empty sample pan was matched with that of the empty reference pan within ±0.2 mg. Samples were heated at a ramp rate of 10 °C/min from 0 to 200 °C with a modulation temperature amplitude of 1 °C/60 s. Data were analyzed using TA Universal Analysis 2000 software (TA Instruments, New Castle, DE).

2.6. Particle size analysis

Particle size distribution, based on volume fraction, of the colloidal dispersions of Wet-milled ITZ and URF–ITZ was measured by static light scattering with a Malvern Mastersizer-S (Malvern Instruments, Ltd., Worcestershire, UK). The colloidal dispersion of URF–ITZ (equivalent to 20 mg ITZ/mL) was prepared by dispersing an aliquot of URF–ITZ powder (~170 mg) in 5 mL purified water by sonication on an ice bath. The colloidal dispersion of Wet-milled ITZ was prepared by dispersing an aliquot of Wet-milled ITZ powder (~100 mg) in 5 mL aqueous solution containing 1% mannitol and 0.4% lecithin to make the compositions same as the URF–ITZ dispersion. The respective dispersion was then diluted with about 500 mL of purified water to produce light obscuration in the range of 10–15%. Values reported are the average of at least three measurements.

2.7. Brunauer–Emmett–Teller (BET) specific surface area analysis

Specific surface area was measured using a Nova 2000 version 6.11 instrument (Quantachrome Instruments, Boynton Beach, FL) with nitrogen as the adsorbate gas. An aliquot of powder was added to a 12-mm Quantachrome bulb sample cell and degassed for a minimum of 8 h prior to analysis. Six points were taken over a range of relative pressures from 0.05 to 0.35. The data were analyzed with the BET equation using NOVA Enhanced Data Reduction Software (version 2.13).

2.8. Dissolution testing under supersaturated conditions

Dissolution testing at supersaturated conditions was conducted in a USP 25 dissolution apparatus model Vankel 7000 Dissolution Tester (Vankel Technology Group, Cary, NC) using 100 mL glass dissolution vessels and stirred with small paddles at 100 rpm. Simulated lung fluid containing 0.02% dipalmitoylphosphatidylcholine [37] was used as the dissolution medium and pre-heated to 37 °C. Aliquots of the URF–ITZ and Wet-milled ITZ colloidal dispersions (equivalent of 80 μg ITZ, equal to 100-times of the equilibrium solubility (C_{eq}) of crystalline ITZ) were added to the dissolution vessels (n = 6), respectively, within 1 s immediately after preparation. Aliquots of 2 mL of the dissolution media were taken at 5, 15, 30 min, 1, 2, 3, 6, 12, and 24 h. The samples were immediately filtered through a 0.2-μm GHP Acrodisc filter (Pall Corporation, East Hills, NY) and diluted with acetonitrile for content analysis. The ITZ content was quantified using a Shimadzu LC-10A high performance liquid chromatography (HPLC) system (Shimadzu Corporation, Columbia, MD). The mobile phase was acetonitrile/water/diethanolamine (70:30:0.05), and it eluted the ITZ peak at approximately 5.5 min at 25 °C with a flow rate of 1 mL/min. The ITZ absorbance was measured at a wavelength λ_{max} of 263 nm. The supersaturation levels are reported as C/C_{eq}. Supersaturation was plotted versus time, and area-under-the-supersaturation-curve (AUSC) was calculated by the linear trapezoidal rule.

2.9. In vitro aerosol performance

An aliquot (5 mL) of the colloidal dispersions of the Wet-milled ITZ and URF–ITZ (equivalent to 20 mg/mL ITZ) was nebulized using an Aeroneb® Professional micropump vibrating mesh nebulizer (Nektar Inc., Mountain View, CA) for about 10 min. The *in vitro* deposition characteristics of the colloidal dispersions of Wet-milled ITZ and URF–ITZ for nebulization were investigated using an eight-stage Andersen cascade impactor (Thermo-Electron Corp., Symrna, GA). The cascade impactor was assembled and operated in accordance with USP General Chapter 601 to assess the drug delivered. The flow rate of the nebulized aerosols was maintained by a vacuum pump (MFG Corp., Benton Harbor, MI) that was calibrated by a TSI mass flowmeter (Model 4000, TSI Inc., St. Paul, MN) to an air flow rate of 28.3 L/min. After deposition onto the stages of the impactor, the mass deposited on each of the impactor pieces was collected and the total mass of drug was quantified by HPLC.

2.10. In vivo pulmonary dosing of rats

With the approval and in accordance with the Institutional Animal Care and Use Committee (IACUC) guidelines at The University of Texas at Austin, *in vivo* studies were conducted using jugular vein pre-catheterized CD® IGS Sprague–Dawley rats (Charles River Laboratories, Inc., Wilmington, MA), weighing 275–325 g. Throughout the study, the rats were housed individually, subjected to 12 h/12 h light and darkness cycles, with access to food and water *ad libitum*. The catheters were flushed daily with heparinized normal saline. After acclimatization for 3 days, eight rats in each formulation group were dosed by inhalation of the nebulized colloidal dispersions of the Wet-milled ITZ and URF–ITZ (equivalent to 20 mg/mL ITZ), respectively, for 10 min in a nose-only dosing apparatus, as shown in Fig. 1. An Aeroneb® Professional micropump nebulizer was situated at the inlet of the dosing tube, and the nebulized drug aerosols go through the dosing tube with an air flow rate of 1 L/min. Following exposure to the aerosol cloud, serial blood samples (approximately 0.3 mL each) were withdrawn through the jugular vein catheter at 0, 0.5, 1, 1.5, 2, 2.5, 3, 4, 6, 8, 12, and 24 h post dosing and placed into a pre-heparinized micro-centrifuge tube. Equal volumes of saline were replaced after each sampling. Two rats in each dosing group were sacrificed immediately upon finishing inhalation to harvest the lungs for determining the lung deposition of the inhaled drug. The lungs of the other rats were harvested at 24 h upon completing blood sampling.

2.11. Plasma and lung analysis

Plasma was separated by centrifugation at 3000*g* for 10 min in a 1.5-mL micro-centrifuge tube using a Microfuge® 18 centrifuge (Beckman Coulter, Fullerton, CA). The plasma and lung samples were stored at −80 °C until HPLC analysis. The lung homogenates were prepared by adding 1 mL of normal saline to a portion of about 0.5 g of the harvested lung and using a homogenizer (Omni International, Marietta, GA) on ice bath. Drug levels in the calibration standards, plasma, and homogenized lung samples were analyzed as the following procedures. Briefly, to an aliquot of 250 μL plasma or 250 μL of lung homogenate, 50 μL of 0.3 N barium

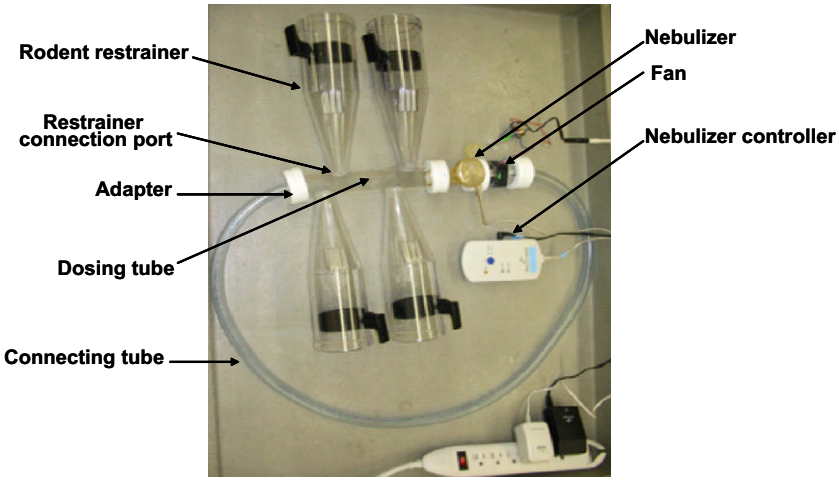

Fig. 1. Picture of the nose-only dosing apparatus for rodents. (For interpretation of the references to colour in this figure legend, the reader is referred to the web version of this article.)

hydroxide and 50 μL of 0.4 N zinc sulfate heptahydrate solutions were added and vortex mixed for 30 s to precipitate water-soluble proteins. Acetonitrile (1 mL) containing 500 ng/mL ketoconazole as an internal reference standard was added to each sample followed by vortex mixing for 1.5 min. Each sample was then centrifuged at 3000*g* for 15 min. The supernatant was transferred to a clean tube and dried under a stream of nitrogen gas. Each sample was reconstituted with 250 μL mobile phase and analyzed by HPLC with wavelength λ_{max} of 263 nm and column maintained at 37 °C. The limit of detection and quantitation for ITZ was 10 ng/mL and 30 ng/mL, respectively. The ITZ peak eluted at approximately 18 min, and the ketoconazole peak eluted at 9.3 min at a flow rate of 1.0 mL/min.

2.12. Pharmacokinetic and statistical analysis

Plots of the log concentration of ITZ in plasma versus time exhibited a first-order absorption phase and a first-order elimination phase. A one-compartmental model for extravascular administration was therefore selected to assess the pharmacokinetic parameters of ITZ in rat plasma using WinNonlin Professional Version 2.1 (Pharsight Corporation, Mountain View, CA). All results are presented as mean ± SD. Student's *t* tests were conducted using SigmaPlot version 7 (Systat Software, Inc., Chicago, IL) to determine the significance between the two dosing groups. For all tests, statistical significance was defined by $p < 0.05$.

3. Results and discussion

3.1. Physicochemical properties of Wet-milled ITZ and URF–ITZ formulations

3.1.1. Morphology and particle size distribution

In the widely used wet milling process, comminution continually fractures drug crystals to reduce the particle size. The efficiency depends upon the nature of the grinding medium, the wetting of the solid, and the hardness of the drugs [38]. In the present study, because of the limited achievable rolling speed of the mill and hardness of ITZ, it took 10 days to reduce the particle size from an average size of 5 μm (100% < 17.7 μm) to nano-size level. The low solubility of ITZ may be advantageous in suppressing crystal growth during and after the milling process, and the hardness (*i.e.* the high melting point) may favor comminution. From the SEM image in Fig. 2a, Wet-milled ITZ was composed of fractured, irregular shaped particles with various sizes, ranging from about 150 to 600 nm in length. This is consistent with a report that NanoCrystals of beclomethsaone dipropiante can be prepared by ball milling a 5% w/w drug suspension in 2.5% PVA over a day, resulting in a mean size of 267 nm [38].

In contrast to Wet-milled ITZ, URF–ITZ powder exhibited a highly porous structure with more regularly round-shaped particles as shown in Fig. 2b. The SEM displayed aggregated nanoparticles that formed a porous matrix. Both the milling and URF process dramatically reduced ITZ particles to nano-size range compared to bulk micron-sized ITZ particles shown in Fig. 2c.

With the particle size reduction, the specific surface area of the Wet-milled ITZ and URF–ITZ powder was found to be 38.6 and 31.7 m^2/g, respectively, which correspond to effective particle diameters of 150 and 190 nm (Table 1), assuming the particles were monodisperse and in spherical shape. The surface area of the bulk ITZ particles of 2.20 m^2/g was 15-times smaller.

However, the particle size distribution analysis using static laser light scattering showed $D(v, 0.5)$ and $D(v, 0.9)$ (diameter at which the cumulative sample volume was under 50% and 90%, respectively) values of 0.57 and 1.22 μm, respectively, for Wet-milled ITZ in colloidal dispersion (Table 1). This value is larger than that inferred from the measured surface area and SEM. Though the primary particle size of Wet-milled ITZ is ~190 nm from the surface area, the potential for increased Van der Waals interactions and electrostatic attraction between ultrafine particles can lead to aggregates ranging from loose flocculates to completely fused particles [13]. It is possible that some of the primary particles formed aggregates that were detected by static light scattering. Nevertheless, over 80% of the particles had a diameter of 1 μm or less.

In comparison, the URF–ITZ colloidal dispersion showed a narrow and smaller range with $D(v, 0.5)$ and $D(v, 0.9)$ of 0.25 and 0.59 μm, respectively. The stable and relatively uniform particle sizes resulted from the rapid nucleation during ice formation in URF and arrested growth as the solution freezes as discussed previously [31].

3.1.2. Crystalline state evaluation

From the XRD diffraction profiles in Fig. 3, ITZ exhibited intense characteristic crystalline peaks at 14.35, 17.46, 20.31, and 23.41 2-theta degrees, as seen in the micron-sized bulk ITZ (as purchased from the manufacturer). The XRD patterns of Wet-milled ITZ were found to be superimposable to the spectra of the micronized crys-

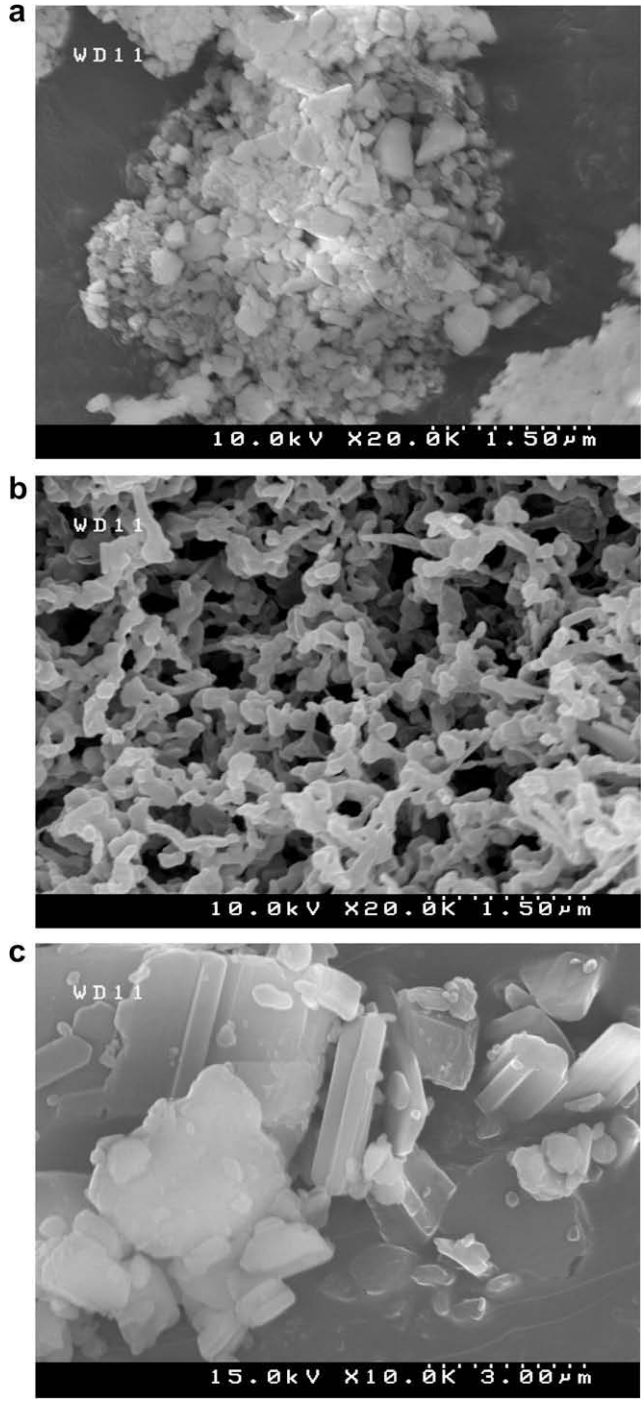

Fig. 2. SEM images of (a) Wet-milled ITZ (wet milling–processed pure ITZ) powder at a magnification of 20 k, (b) URF–ITZ (URF-processed ITZ/mannitol/lecithin = 1:0.5:0.2, weight ratio) powder at a magnification of 20 k, and (c) bulk ITZ as received at a magnification of 10 k.

talline ITZ but with smaller peak heights. Reducing particle size can result in XRD peak broadening and halo formation, due to lost long-range crystalline order, without complete transition to an amorphous form [39]. It was also reported that XRD profiles of asulacrine nanocrystals with a mean particle size of 130 nm made by high-pressure homogenization were not affected, with similar peak intensities as for micron-sized drug [20]. The XRD patterns of nanocrystal therefore seem material-specific and are related to the crystalline microstructure (crystal size, micro-strain and defects) of individual substances [39]. Therefore, the reduction in

Table 1
Particle size distributions, specific surface areas (SSA), and the calculated particle sizes based on SSA of Wet-milled ITZ (wet milling–processed pure ITZ) and URF–ITZ (URF-processed ITZ/mannitol/lecithin = 1:0.5:02) powders.

Samples	Particle size (μm)			Specific surface area (m^2/g)	Calculated particle size (μm)
	$D(v, 0.1)$	$D(v, 0.5)$	$D(v, 0.9)$		
Wet-milled ITZ	0.16	0.57	1.22	31.7	0.19
URF–ITZ	0.10	0.25	0.59	38.6	0.15

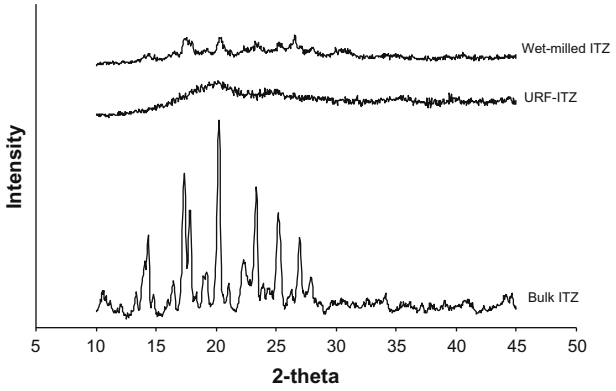

Fig. 3. X-ray powder diffraction patterns (from the top to bottom): Wet-milled ITZ (wet milling–processed pure ITZ), URF–ITZ (URF-processed ITZ/mannitol/Lecithin = 1:0.5:0.2), micronized bulk ITZ.

XRD peak intensity of Wet-milled ITZ is most likely due to particle size reduction.

For XRD of URF–ITZ powder in Fig. 3, broad, diffuse haloes were present with an absence of the characteristic crystalline peaks, indicating a highly amorphous morphology [25]. The crystallinity was examined further with MTDSC as shown in Fig. 4. The URF–ITZ powder exhibited a glass transition at around 50 °C, one exothermic recrystallization peak, and finally a single endothermic melting peak at 165.7 °C. These results further confirmed the amorphous nature of URF–ITZ seen by XRD. In contrast, an exothermic peak was not present for Wet-milled ITZ, but only a single endothermic peak at 163.4 °C, corresponding to the melting of ITZ. However, the melting peak of Wet-milled ITZ was not as sharp as for bulk ITZ and shifted slightly.

Milling processes may generate amorphous domains on the particle surface [40]. Despite the long time period for milling the ITZ, the crystallinity was high and the amorphous content undetectable according to the XRD and DSC results.

3.2. Supersaturation of Wet-milled ITZ and URF–ITZ colloidal dispersions in simulated lung fluid

Dissolution of the ITZ colloidal dispersions in simulated lung fluid with pH 7.4 at 37 °C was conducted under supersaturated conditions (100-times C_{eq} equivalent ITZ were added) as shown in Fig. 5. The C_{eq} in simulated lung fluid was measured to be 8 ng/mL after shaking at 37 °C for 3 days with excess bulk ITZ present. For the URF-ITZ, C/C_{eq} reached 22-times at 5 min and a maximum value of about 26-times at 15 and 30 min. The supersaturation levels gradually decreased to about 7-times at 2 h, and 5-times at 24 h. In contrast, the supersaturation for Wet-milled ITZ only reached about 3-times the measured C/C_{eq} at 30 min, fell to about 2-times at 6 h and then gradually declined to about the equilibrium ratio at 24 h. The cumulative extent of supersaturation was calculated as the AUSC, which was 1785 and 383 ng h/mL for URF–ITZ and Wet-milled ITZ, respectively. The

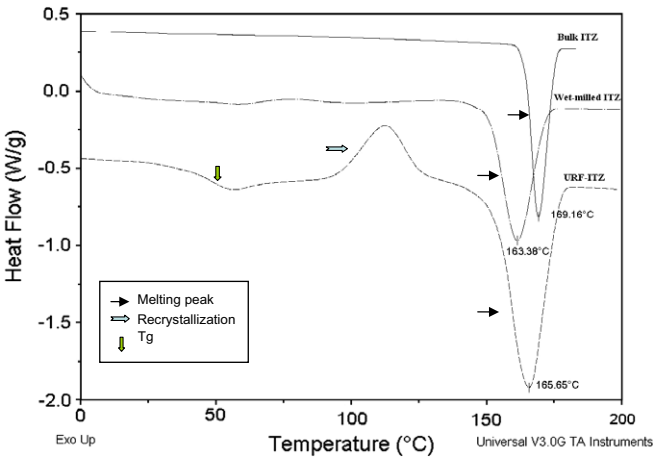

Fig. 4. DSC profiles of bulk ITZ, Wet-milled ITZ (wet milling–processed pure ITZ) powder and URF–ITZ (URF-processed ITZ/mannitol/lecithin = 1:0.5:0.2, weight ratio) powder. (For interpretation of the references to colour in this figure legend, the reader is referred to the web version of this article.)

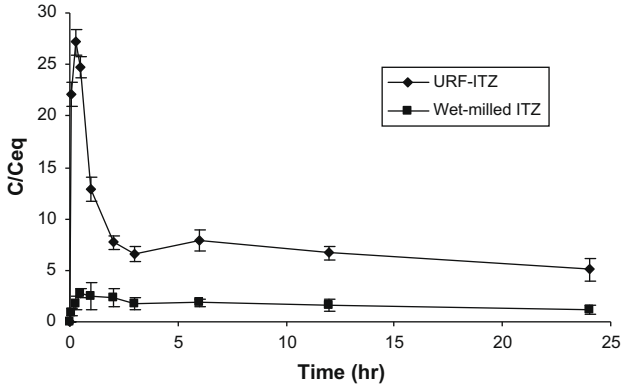

Fig. 5. Dissolution profiles of Wet-milled ITZ colloidal dispersion (ITZ/mannitol/lecithin = 1:0.5:0.2, weight ratio) and URF–ITZ colloidal dispersion (ITZ/mannitol/lecithin = 1:0.5:0.2, weight ratio) in simulated lung fluid (pH = 7.4) at supersaturation conditions (*i.e.* 100-times equilibrium solubility of micronized crystalline ITZ was added) using 100-mL vessels and small paddle apparatus at 100 rpm and 37 °C.

much larger C_{sat} at various times and AUSC for the amorphous URF–ITZ have the potential to enhance bioavailability of this poorly water-soluble drug.

Formation of a high energy amorphous or semicrystalline state can increase the predicted solubility, in many cases up to 100-times that of its crystalline form [23,28]. The URF–ITZ formulation has been previously identified to be a solid solution of ITZ molecularly dispersed in mannitol and lecithin matrix [31]. Once the solid solution was exposed to the aqueous simulated lung fluid, the excipients dissolved very rapidly and the high surface area ITZ domains quickly supersaturated the dissolution medium. Because of the maximal achievable surface area for dissolution obtained by solid solution [41], the dissolution rate and C_{sat} value of URF–ITZ colloidal dispersion could be much higher than Wet-milled ITZ colloidal dispersion upon added to a dissolution medium. The elevated C_{sat} value of URF–ITZ might therefore be responsible for the 4.7-times higher amount of solvated ITZ molecules in the simulated lung fluid than Wet-milled ITZ.

The driving force for dissolution depends on the drug solubility within a given environment (*i.e.* lung fluid) C_{sat} and the concentration gradient between C_{sat} at the particle surface and C in the bulk solution phase. Particle dissolution is governed by several factors that can be described by the Noyes–Whitney equation:

$$dM/dt = AD(C_{sat} - C)/h$$

where dM/dt is the fraction of mass dissolved per unit time, A is the surface area available for dissolution, D is the diffusion coefficient, and h is the thickness of the diffusion boundary layer. Nanoparticles often dissolve more quickly due to the extensive enhancement in surface area, the smaller h which is proportional to the particle diameter and the higher C_{sat} because of particle curvature according to the Kelvin equation [42]. The nano-sized URF–ITZ and Wet-milled ITZ both dissolved rapidly and reached a maximum concentration within 30 min, as well as supersaturation relative to equilibrium solubility of the micronized ITZ. The D value was the same for both formulations, and the available surface areas A were similar. Also, the h values which are closely related to particle size [43] were similar. Thus, the higher dissolution rate for the amorphous ITZ is due to the higher C_{sat} values.

3.3. In vitro aerosol performance of Wet-milled ITZ and URF–ITZ aqueous colloidal dispersions

Pulmonary drug delivery targeted to the alveoli is advantageous and critical for systemic absorption [44], as the distance from the air in the alveolar lumen to the capillary blood flow is less than 400 nm [45]. The efficacy of pulmonary delivery of drug to the deep lung is largely determined by the particle size distribution of aerosol droplets [46]. The inhaled aerosol should possess a narrow range of aerodynamic diameters between 1 and 5 μm to pass through the filter of the mouth and throat to be effectively delivered inside the lung [22]. The aerosolization behavior was described in terms of total emitted dose (TED), mass median aerodynamic diameter (MMAD), geometric standard deviation (GSD), and percentage fine particle fraction (FPF), as summarized in Table 2. The TED of Wet-milled ITZ and URF–ITZ was 51.7 and 56.4 mg out of 100 mg ITZ available for nebulization, respectively. Their corresponding FPF were 47.3% and 54.4% with the respective fine particle dose (defined as the amount of aerosol droplets entering the impactor less than 4.7 μm, TED × FPF, indication of the dose delivered to the deep lung) delivered at a rate of 2.45 and 3.07 mg/min. The MMAD of the atomized droplets of Wet-milled ITZ and URF–ITZ colloidal dispersions were 2.8 and 2.4 μm with GSD of 3.1 and 2.7, respectively, which are suitable for deep lung delivery.

In this study, the aerodynamic diameter is governed by the easily controllable nebulization of the aqueous droplets, which contain much smaller dispersed particles of drug. It was reported that the Aeroneb® Professional micropump nebulizer produced an aqueous mist of fine droplets with sizes ranging between 1 and 4 μm [33]. Nanoparticles with a diameter of less than 1 μm are more easily incorporated in the respirable aerosolized droplets with MMAD of 1–5 μm [47]. Furthermore, the viscosities of the col-

Table 2
Cascade impaction data for nebulized aerosols of Wet-milled ITZ colloidal dispersion (ITZ/mannitol/lecithin = 1:0.5:0.2, weight ratio) and URF–ITZ colloidal dispersion (ITZ/mannitol/lecithin = 1:0.5:0.2, weight ratio) (equivalent to 100 mg of total ITZ), using the Aeroneb Professional micropump nebulizer at an air flow rate of 28.3 L/min for 10 min.

	Wet-milled ITZ	URF–ITZ
Total emitted dose (mg)	51.7	56.4
Respirable fraction[a] (%)	74.5	73.0
Fine particle fraction[b] (%)	47.3	54.4
Available dose (mg/min)	3.86	4.11
Mass median aerodynamic diameter (MMAD) (μm)	2.8	2.4
Geometric standard deviation (GSD)	3.1	2.7

[a] Defined as the % mass of drug in aerosol droplets <9 μm.
[b] Defined as the % mass of drug in aerosol droplets <4.7 μm.

loidal dispersions are similar to those of the water. The low viscosity facilitates the formation of small and uniform droplets [48]. Since both URF–ITZ and Wet-milled ITZ colloidal dispersions contain submicron particles, the aerodynamic performance of the nebulized fine aerosol droplets is similar to that of pure water.

3.4. Pharmacokinetics of inhaled Wet-milled ITZ and URF–ITZ in rats

With the same compositions and comparable *in vitro* aerodynamic performance of the nebulized aerosols of Wet-milled ITZ and URF–ITZ colloidal dispersions, their *in vivo* performance was subsequently explored in a rat model. Rats were exposed nose-only to a single-dose aerosol of the nebulized colloidal dispersions (equivalent to 100 mg of ITZ total), respectively, for about 10 min. Drug concentration profiles in lung tissue and blood following a single-inhalation dose are presented in Figs. 6 and 7. Upon completing inhalation of the nebulized compositions (0 h post dosing), 12.28 ± 0.60 and 11.01 ± 4.26 μg/g wet lung weight of ITZ were found deposited in lungs from Wet-milled ITZ and URF–ITZ dosing groups, respectively. At 24 h post dosing, these values were 0.56 ± 0.44 and 0.46 ± 0.24 μg/g wet lung weight, respectively.

Once deposited in the lungs, the nanoparticles underwent dissolution in the lung lining fluid to release free ITZ molecules for local lung action or were further absorbed through lung alveolar epithelium to systemic circulation. The corresponding pharmacokinetic parameters in blood are summarized in Table 3. In plasma, based on a one-compartmental analysis, the C_{max} for Wet-milled ITZ and URF–ITZ dosing group were 50 and 180 ng/mL at 2.7 and 4.0 h after dosing, respectively. The AUC_{0-24} of Wet-milled ITZ and URF–ITZ was 662 and 2543 ng h/mL, respectively. In URF–ITZ dosing group, after reaching the C_{max}, a plateau of the high ITZ level was maintained from 2.5 to 6.0 h, similar to a sustained release profile. At all the sampling time points, the ITZ levels in rats inhaled URF–ITZ were significantly higher than those inhaled Wet-milled ITZ.

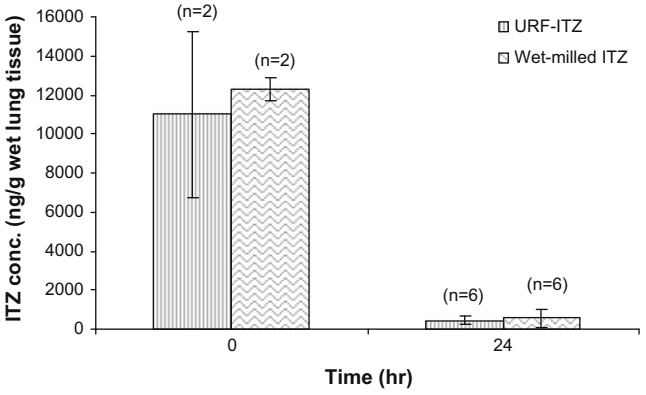

Fig. 6. Lung deposition of ITZ in rats at 0 and 24 h post inhalation of a single-dose nebulized aqueous Wet-milled ITZ colloidal dispersion (ITZ/mannitol/lecithin = 1:0.5:0.2, weight ratio) and URF-ITZ colloidal dispersion (ITZ/mannitol/lecithin = 1:0.5:0.2, weight ratio). Data are presented as Mean ± SD.

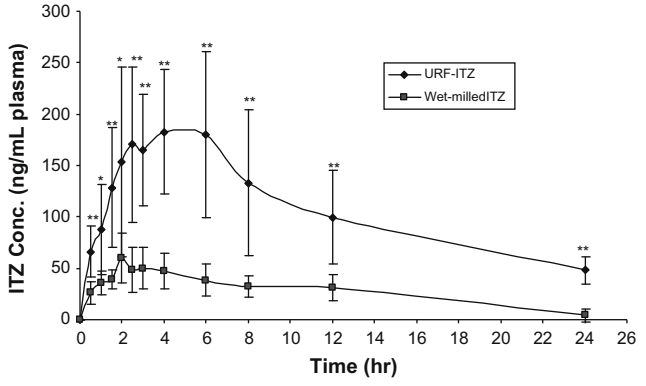

Fig. 7. Plasma concentration of ITZ in rats after a single-dose inhalation of nebulized aqueous Wet-milled ITZ colloidal dispersion (ITZ/mannitol/lecithin = 1:0.5:0.2, weight ratio) and URF–ITZ colloidal dispersion (ITZ/mannitol/lecithin = 1:0.5:0.2, weight ratio). Data are presented as Mean ± SD, $n = 6$. $^{*}p < 0.05$, $^{**}p < 0.01$.

Despite the comparable lung deposition levels of the inhaled aerosols of the two ITZ colloidal dispersions, the cumulative ITZ concentrations absorbed into blood from rats was about 3.8-times higher for the URF–ITZ versus Wet-milled ITZ. From Fick's first law, the systemic absorption rate of a drug from the lung epithelium is given by $P \times A \times C$, where P is membrane permeability, A is the available surface area over which the drug is spread, C is the drug concentration in the lung lining fluids. The drug concentration in blood is assumed to be insignificant compared to the lung concentration and the transfer from lung to blood is irreversible [49]. For the Wet-milled ITZ and URF–ITZ colloidal dispersions, many factors were fairly constant including the composition, aerodynamic performance, lung depositions, total drug dose, permeability and absorption area. The absorption has been shown to be permeation limited for both amorphous and crystalline ITZ nanoparticles of the sizes on the order of 200–600 nm with a combined dissolution/permeation material balance in the lung fluid [31]. Here the dissolution is essentially instantaneous relative to the permeation. In this case, the flux of ITZ into systemic circulation would be directly proportional to the dissolved concentration C_{sat}. This prediction was observed in the current study. The 3.8-times larger AUC of URF–ITZ in the systemic circulation versus Wet-milled ITZ was on the same order as the 4.7-times larger supersaturation level (thermodynamic activity) measured in the *in vitro* dissolution test.

The biopharmaceutical consequences of solubility differences of polymorphs are directly related to the solubility difference [50]. It was reported that polymorphs of chloramphenicol palmitate with a measured solubility ratio of about 4.0 induced about 6-times difference in C_{max} in human after oral administration [51], whereas no significant difference in pharmacokinetics was observed after a single oral dose of polymorphs of mefenamic acid with measured solubility ratio of about 1.3 [50]. Therefore, to achieve clinically meaningful biopharmaceutical consequences of solubility differences, the solubility ratios need to be about twofold higher [23]. Compared to the crystalline counterpart, the formation of significantly higher levels of supersaturation offered by amorphous formulations of drugs with poor/erratic bioavailability enhances total drug absorption (AUC) and C_{max} while reducing t_{max} as observed for oral [52], topical [53], and pulmonary [54] administrations. The use of amorphous form of poorly water-soluble drugs has widened the window of achievable pharmacokinetic performance enormously.

Table 3
Pharmacokinetic parameters for plasma ITZ concentration in rats after a single-dose inhalation of nebulized aerosols of Wet-milled ITZ colloidal dispersion (ITZ/mannitol/lecithin = 1:0.5:0.2, weight ratio) and URF–ITZ colloidal dispersion (ITZ/mannitol/lecithin = 1:0.5:0.2, weight ratio).

Pharmacokinetic parameters	Wet-milled ITZ	URF–ITZ
C_{max} (ng/mL)	50	180
T_{max} (h)	2.7	4.0
$K_{01\ absorption}$ (/h)	0.98	0.55
$K_{10\ elimination}$ (/h)	0.09	0.08
$T_{1/2\ absorption}$ (h)	0.7	1.3
$T_{1/2\ elimination}$ (h)	7.8	8.2
AUC_{0-24} (ng h/mL)	662	2543

3.5. Lung clearance of the deposited nanoparticles containing ITZ

In addition to influencing aerosol deposition and dissolution in the lung lining fluid, particle size distribution and morphology also may influence the clearance mechanism [40,55]. The lungs have very efficient clearance mechanisms for foreign particles. The MMAD of Wet-milled ITZ and URF–ITZ aerosols favor deposition in the deep lung, bypassing the mucociliary clearance in the airways. Compared to Wet-milled ITZ, the deposited amorphous URF–ITZ nanoparticles dissolve more quickly upon exposure to the lung lining fluid. Furthermore, the rapid dissolution may minimize crystallization of undissolved particles of URF–ITZ in the lung fluid, which would otherwise lower the supersaturation [56]. The more rapid dissolution and resulting higher supersaturation with minimal time for crystallization of undissolved solid results in reduced clearance of URF–ITZ relative to Wet-milled ITZ particles by the lung defense system. These factors favor the observed significantly enhanced bioavailability of URF–ITZ.

For those deposited particles that have not completely dissolved, they would mainly be cleared from the alveoli via endocytosis by epithelial and endothelial cells and phagocytosis by macrophages [57]. The efficiency of clearance of the inhaled particles is size dependent. Alveolar macrophage preferentially uptake particles of approximately 1–3 μm in diameter [22]. Phagocytosis of 1-μm particles has been observed as early as 15 min after nebulization [58]. Furthermore, 30–60% of 1- to 3-μm particles have been observed to be phagocytosed 2–4 h post intra-tracheal instillation, with complete pulmonary clearance of particles within 24 h [59]. After 24-h post inhalation, the ITZ levels in the lung were similar for the URF–ITZ and Wet-milled ITZ, even though the former was absorbed at a level of ∼4-times higher. Thus, the much larger amount of unabsorbed Wet-milled ITZ particles must have been cleared by the lung defense system. The aggregates of the Wet-milled ITZ of 590 nm in mean diameter measured by light scattering are more vulnerable to uptake by macrophage clearance than the smaller URF–ITZ particles, so that ITZ levels in lung at 24-h post inhalation were both significantly reduced.

4. Conclusion

For an aqueous colloidal dispersion of amorphous nanoparticulate ITZ, rapid dissolution produced a supersaturation ∼4.7-times larger than for a dispersion of crystalline nanoparticulates made by wet milling with the same composition and similar particle surface area. The aerodynamic diameters for both dispersions were suitable for deep lung delivery by nebulization, and similar to values produced for pure water. However, the increase in the systemic bioavailability for the amorphous versus crystalline dispersion of about 3.8 was approximately the same as the increase in supersaturation measured *in vitro* in the simulated lung fluid. The experimentally observed similarity in the values of bioavailability and supersaturation would be predicted for a permeability controlled model, where dissolution is very rapid, as suggested previously [31]. The high supersaturation, favored by rapid dissolution of amorphous nanoparticles, prior to particle clearance or crystallization favors the high permeability into the bloodstream. Pulmonary delivery of amorphous nanoparticle formulations of extremely poorly water-soluble drugs, especially for high-dose drugs (e.g. ITZ), is thus beneficial for both local and systemic therapy.

Acknowledgements

This material is supported in part by the STC Program of the National Science Foundation under Agreement No. CHE987664. We would like to thank Mr. Kevin O'Donnell for his assistance with animal study.

References

[1] C.A. Lipinski, Drug-like properties and the causes of poor solubility and poor permeability, Journal of Pharmacological and Toxicological Methods 44 (1) (2000) 235–249.
[2] C.A. Lipinski, F. Lombardo, B.W. Dominy, P.J. Feeney, Experimental and computational approaches to estimate solubility and permeability in drug discovery and development settings, Advanced Drug Delivery Reviews 23 (1–3) (1997) 3–25.
[3] R.H. Muller, C. Jacobs, O. Kayser, Nanosuspensions as particulate drug formulations in therapy rationale for development and what we can expect for the future, Advanced Drug Delivery Reviews 47 (1) (2001) 3–19.
[4] V.B. Patravale, A.A. Date, R.M. Kulkarni, Nanosuspensions: a promising drug delivery strategy, Journal of Pharmacy and Pharmacology 56 (7) (2004) 827–840.
[5] S. Agharkar, S. Lindenbaum, T. Higuchi, Enhancement of solubility of drug salts by hydrophilic counterions – properties of organic salts of an antimalarial drug, Journal of pharmaceutical sciences 65 (5) (1976) 747–749.
[6] K. Amin, R.M. Dannenfelser, J. Zielinski, B. Wang, Lyophilization of polyethylene glycol mixtures, Journal of pharmaceutical sciences 93 (9) (2004) 2244–2249.
[7] V.P. Torchilin, Micellar nanocarriers: pharmaceutical perspectives, Pharmaceutical Research 24 (1) (2007) 1–16.
[8] R.A. Rajewski, V.J. Stella, Pharmaceutical applications of cyclodextrins. 2. In vivo drug delivery, Journal of Pharmaceutical Sciences 85 (11) (1996) 1142–1169.
[9] R. Liu, Water-insoluble Drug Formulation, CO Interpharm Press, Englewood, 2000.
[10] D.J.W. Grant, H.G. Brittian, Physical Characterisation of Pharmaceutical Solids, Marcel Dekker, New York, 1995.
[11] R.J. Hintz, K.C. Johnson, The effect of particle-size distribution on dissolution rate and oral absorption, International Journal of Pharmaceutics 51 (1) (1989) 9–17.
[12] P. Borm, F.C. Klaessig, T.D. Landry, B. Moudgil, J. Pauluhn, K. Thomas, R. Trottier, S. Wood, Research strategies for safety evaluation of nanomaterials, part V: role of dissolution in biological fate and effects of nanoscale particles, Toxicological Sciences 90 (1) (2006) 23–32.
[13] N. Blagden, M. de Matas, P.T. Gavan, P. York, Crystal engineering of active pharmaceutical ingredients to improve solubility and dissolution rates, Advanced Drug Delivery Reviews 59 (7) (2007) 617–630.
[14] G.G. Liversidge, K.C. Cundy, Particle-size reduction for improvement of oral bioavailability of hydrophobic drugs. 1. Absolute Oral bioavailability of nanocrystalline danazol in beagle dogs, International Journal of Pharmaceutics 125 (1) (1995) 91–97.
[15] R. Mauludin, R.H. Muller, C.M. Keck, Development of an oral rutin nanocrystal formulation, International Journal of Pharmaceutics 370 (1–2) (2009) 202–209.
[16] P.C. Chiang, J.W. Alsup, Y.R. Lai, Y.D. Hu, B.R. Heyde, D. Tung, Evaluation of aerosol delivery of nanosuspension for pre-clinical pulmonary drug delivery, Nanoscale Research Letters 4 (3) (2009) 254–261.
[17] W.K. Kraft, B. Steiger, D. Beussink, J.N. Quiring, N. Fitzgerald, H.E. Greenberg, S.A. Waldman, The pharmacokinetics of nebulized nanocrystal budesonide suspension in healthy volunteers, Journal of Clinical Pharmacology 44 (1) (2004) 67–72.
[18] M.A. Kassem, A.A.A. Rahman, M.M. Ghorab, M.B. Ahmed, R.M. Khalil, Nanosuspension as an ophthalmic delivery system for certain glucocorticoid drugs, International Journal of Pharmaceutics 340 (1–2) (2007) 126–133.
[19] R. Pignatello, C. Bucolo, P. Ferrara, A. Maltese, A. Puleo, G. Puglisi, Eudragit RS100 (R) nanosuspensions for the ophthalmic controlled delivery of ibuprofen, European Journal of Pharmaceutical Sciences 16 (1–2) (2002) 53–61.
[20] S. Ganta, J.W. Paxton, B.C. Baguley, S. Garg, Formulation and pharmacokinetic evaluation of an asulacrine nanocrystalline suspension for intravenous delivery, International Journal of Pharmaceutics 367 (1–2) (2009) 179–186.
[21] J.E. Kipp, The role of solid nanoparticle technology in the parenteral delivery of poorly water-soluble drugs, International Journal of Pharmaceutics 284 (1–2) (2004) 109–122.
[22] H.M. Courrier, N. Butz, T.F. Vandamme, Pulmonary drug delivery systems: recent developments and prospects, Critical Reviews in Therapeutic Drug Carrier Systems 19 (4–5) (2002) 425–498.
[23] B.C. Hancock, M. Parks, What is the true solubility advantage for amorphous pharmaceuticals?, Pharmaceutical Research 17 (4) (2000) 397–404
[24] B.C. Hancock, G. Zograf, Characteristics and significance of the amorphous state in pharmaceutical systems, Journal of pharmaceutical sciences 86 (1) (1997) 1–12.
[25] L.R. Hilden, K.R. Morris, Physics of amorphous solids, Journal of Pharmaceutical Sciences 93 (1) (2004) 3–12.
[26] G.V. Betageri, K.R. Makarla, Enhancement of dissolution of glyburide by solid dispersion and lyophilization techniques, International Journal of Pharmaceutics 126 (1–2) (1995) 155–160.
[27] M.E. Matteucci, M.A. Miller, R.O. Williams, K.P. Johnston, Highly supersaturated solutions of amorphous drugs approaching predictions from

configurational thermodynamic properties, Journal of Physical Chemistry B 112 (51) (2008) 16675–16681.
[28] P. Gupta, G. Chawla, A.K. Bansal, Physical stability and solubility advantage from amorphous celecoxib: the role of thermodynamic quantities and molecular mobility, Molecular Pharmaceutics 1 (6) (2004) 406–413.
[29] M.E. Matteucci, B.K. Brettmann, T.L. Rogers, E.J. Elder, R.O. Williams, K.P. Johnston, Design of potent amorphous drug nanoparticles for rapid generation of highly supersaturated media, Molecular Pharmaceutics 4 (5) (2007) 782–793.
[30] J.M. Tam, J.T. McConville, R.O. Williams 3rd, K.P. Johnston, Amorphous cyclosporin nanodispersions for enhanced pulmonary deposition and dissolution, Journal of Pharmaceutical Sciences (2008), doi:10.1002/jps.21367.
[31] W. Yang, J. Tam, D.A. Miller, J. Zhou, J.T. McConville, K.P. Johnston, R.O. Williams, High bioavailability from nebulized itraconazole nanoparticle dispersions with biocompatible stabilizers, International Journal of Pharmaceutics 361 (1–2) (2008) 177–188.
[32] J.M. Vaughn, J.T. McConville, D. Burgess, J.I. Peters, K.P. Johnston, R.L. Talbert, R.O. Williams 3rd, Single dose and multiple dose studies of itraconazole nanoparticles, European Journal of Pharmaceutics and Biopharmaceutics 63 (2) (2006) 95–102.
[33] J.T. McConville, K.A. Overhoff, P. Sinswat, J.M. Vaughn, B.L. Frei, D.S. Burgess, R.L. Talbert, J.I. Peters, K.P. Johnston, R.O. Williams, Targeted high lung concentrations of itraconazole using nebulized dispersions in a murine model, Pharmaceutical Research 23 (5) (2006) 901–911.
[34] B.J. Hoeben, D.S. Burgess, J.T. McConville, L.K. Najvar, R.L. Talbert, J.I. Peters, N.P. Wiederhold, B.L. Frei, J.R. Graybill, R. Bocanegra, K.A. Overhoff, P. Sinswat, K.P. Johnston, R.O. Williams, In vivo efficacy of aerosolized nanostructured itraconazole formulations for prevention of invasive pulmonary aspergillosis, Antimicrobial Agents and Chemotherapy 50 (4) (2006) 1552–1554.
[35] J. Peeters, P. Neeskens, J.P. Tollenaere, P. Van Remoortere, M.E. Brewster, Characterization of the interaction of 2-hydroxypropyl-beta-cyclodextrin with itraconazole at pH 2, 4, and 7, J Pharm Sci 91 (6) (2002) 1414–1422.
[36] K.A. Overhoff, J.D. Engstrom, B. Chen, B.D. Scherzer, T.E. Milner, K.P. Johnston, R.O. Williams 3rd, Novel ultra-rapid freezing particle engineering process for enhancement of dissolution rates of poorly water-soluble drugs, European Journal of Pharmaceutics and Biopharmaceutics 65 (1) (2007) 57–67.
[37] R.O. Cook, R.K. Pannu, I.W. Kellaway, Novel sustained release microspheres for pulmonary drug delivery, Journal of Controlled Release 104 (1) (2005) 79–90.
[38] T.S. Wiedmann, L. DeCastro, R.W. Wood, Nebulization of nanocrystals(TM): production of a respirable solid-in-liquid-in-air colloidal dispersion, Pharmaceutical Research 14 (1) (1997) 112–116.
[39] Z. Deng, S. Xu, S. Li, Understanding a relaxation behavior in a nanoparticle suspension for drug delivery applications, International Journal of Pharmaceutics 351 (1–2) (2008) 236–243.
[40] A.H.L. Chow, H.H.Y. Tong, P. Chattopadhyay, B.Y. Shekunov, Particle engineering for pulmonary drug delivery, Pharmaceutical Research 24 (3) (2007) 411–437.
[41] C. Leuner, J. Dressman, Improving drug solubility for oral delivery using solid dispersions, European Journal of Pharmaceutics and Biopharmaceutics 50 (1) (2000) 47–60.
[42] M.T. Crisp, C.J. Tucker, T.L. Rogers, R.O. Williams 3rd, K.P. Johnston, Turbidimetric measurement and prediction of dissolution rates of poorly soluble drug nanocrystals, Journal of Controlled Release 117 (3) (2007) 351–359.
[43] A.P. Tinke, K. Vanhoutte, R. De Maesschalck, S. Verheyen, H. De Winter, A new approach in the prediction of the dissolution behavior of suspended particles by means of their particle size distribution, Journal of Pharmaceutical and Biomedical Analysis 39 (5) (2005) 900–907.
[44] H.M. Courrier, N. Butz, T.F. Vandamme, Pulmonary drug delivery systems: recent developments and prospects, Critical Reviews in Therapeutic Drug Carrier Systems 19 (4–5) (2002) 425–498.
[45] R. Altiere, D. Thompson, in: A. Hickey (Ed.), Inhalation Aerosols–Physical and Biological Basis for Therapy, Marcel Dekker, Inc., New York, 1996, pp. 85–138.
[46] T.B. Martonen, I.M. Katz, Deposition patterns of aerosolized drugs within human lungs – effects of ventilatory parameters, Pharmaceutical Research 10 (6) (1993) 871–878.
[47] L.A. Dailey, T. Schmehl, T. Gessler, M. Wittmar, F. Grimminger, W. Seeger, T. Kissel, Nebulization of biodegradable nanoparticles: impact of nebulizer technology and nanoparticle characteristics on aerosol features, Journal of Controlled Release 86 (1) (2003) 131–144.
[48] B.Y. Shekunov, P. Chattopadhyay, D. Yim, D. Cippola, B. Boyd, Formulation and in vitro performance of drug-lipid nanosuspensions for pulmonary delivery, in: Conference on Respiratory Drug Delivery, Boca Raton, Florida, 2006, pp. 609–612.
[49] J.S. Patton, P.R. Byron, Inhaling medicines: delivering drugs to the body through the lungs, Nature Reviews 6 (1) (2007) 67–74.
[50] A.J. Aguiar, J.E. Zelmer, Dissolution behavior of polymorphs of chloramphenicol palmitate and mefenamic acid, Journal of Pharmaceutical Sciences 58 (8) (1969) 983–987.
[51] A.J. Aguiar, J. Krc Jr., A.W. Kinkel, J.C. Samyn, Effect of polymorphism on the absorption of chloramphenicol from chloramphenicol palmitate, Journal of Pharmaceutical Sciences 56 (7) (1967) 847–853.
[52] D.A. Miller, J.T. McConville, W. Yang, R.O. Williams 3rd, J.W. McGinity, Hot-melt extrusion for enhanced delivery of drug particles, Journal of Pharmaceutical Sciences 96 (2) (2007) 361–376.
[53] V. Sanna, E. Gavini, M. Cossu, G. Rassu, P. Giunchedi, Solid lipid nanoparticles (SLN) as carriers for the topical delivery of econazole nitrate: in-vitro characterization, ex-vivo and in-vivo studies, Journal of Pharmacy and Pharmacology 59 (8) (2007) 1057–1064.
[54] P. Sinswat, K.A. Overhoff, J.T. McConville, K.P. Johnston, R.O. Williams, Nebulization of nanoparticulate amorphous or crystalline tacrolimus – single-dose pharmacokinetics study in mice, European Journal of Pharmaceutics and Biopharmaceutics 69 (3) (2008) 1057–1066.
[55] W. Yang, J.I. Peters, R.O. Williams, Inhaled nanoparticles – a current review, International Journal of Pharmaceutics 356 (1–2) (2008) 239–247.
[56] M.E. Matteucci, J.C. Paguio, M.A. Miller, R.O. Williams, K.P. Johnston, Highly supersaturated solutions from dissolution of amorphous itraconazole microparticles at pH 6.8, Molecular Pharmaceutics 6 (2) (2009) 375–385.
[57] A. Nemmar, H. Vanbilloen, M.F. Hoylaerts, P.H. Hoet, A. Verbruggen, B. Nemery, Passage of intratracheally instilled ultrafine particles from the lung into the systemic circulation in hamster, American Journal of Respiratory and Critical Care Medicine 164 (9) (2001) 1665–1668.
[58] P. Forsgren, J. Modig, B. Gerdin, B. Axelsson, M. Dahlback, Intrapulmonary deposition of aerosolized evans blue-dye and liposomes in an experimental porcine model of early Ards, Upsala Journal of Medical Sciences 95 (2) (1990) 117–136.
[59] H.Y. Zhou, Y.L. Zhang, D.L. Biggs, M.C. Manning, T.W. Randolph, U. Christians, B.M. Hybertson, K.Y. Hg, Microparticle-based lung delivery of INH decreases INH metabolism and targets alveolar macrophages, Journal of Controlled Release 107 (2) (2005) 288–299.